RESEARCH ARTICLE

Macromolecular Rapid Communications
www.mrc-journal.de

Linker Group Fluorination Boosts Photovoltaic Performance of Branch-Connected Dimerized Acceptors

Yuxin Wang, Xinyuan Jia, Kangqiao Ma, Wenkai Zhao, Huazhe Liang, Zhaoyang Yao, Guankui Long, Chenxi Li, Xiangjian Wan, and Yongsheng Chen**

Branch-connected dimerized acceptors can take full advantages of four end units in enhancing molecular packing comparing to that of terminal-connected ones, thus potentially reaching the best balance between stability and power conversion efficiency (PCE) of organic solar cells (OSCs). Herein, two branch-connected dimerized acceptors, namely D1 and D2, are developed by employing bithiophene and difluorinated bithiophene as linker groups, respectively. Induced by the fluorine atoms on linker group, D2 affords a larger molar extinction coefficient, more importantly, the optimized nanoscale film morphology and superior charge transport behavior comparing to D1. Consequently, D2-based binary OSCs render a good PCE of 16.66%, outperforming that of 15.08% for D1-based ones. This work highlights the great significance of linker group screening in designing high-performance branch-connected dimerized acceptors.

1. Introduction

Organic solar cells (OSCs), as a promising photovoltaic technology, have been paid enormous attention due to their intrinsic lightweight, excellent flexibility, and low-cost characteristics.[1–4] In recent years, with the great development of acceptor–donor–acceptor type small molecular acceptors (SMAs), OSCs have achieved outstanding power conversion efficiencies (PCEs) exceeding 20%,[5–9] however, are still faced with the great challenge of long-term operational stability.[10–12] Among the multiple factors, a determining one may be the diffusion of SMAs from a dynamic equilibrium state to a thermodynamic state.[13–15] To address this issue, polymerized SMAs (PSMAs) have been proposed by Li et al., and indeed revealed better stability of OSCs according to lots of systematic investigations.[16–18] Currently, all-polymer solar cells have reached PCEs over 19%.[19–21] Nevertheless, compared to SMAs with a definite structure, PSMAs generally suffer from batch-to-batch variations,[22–24] which limits their potential in the practical application of OSCs. Therefore, by combining the advantages of clear structure for SMAs and high glass transition temperature for PSMAs, dimerized acceptors come into being, exhibiting great potential in the industrialization of organic photovoltaics.[25–27]

At present, most of the dimerized SMAs were constructed by coupling the electron-withdrawing terminal of SMAs with a linker group.[28–30] This type of connection usually leads to some defects. First of all, the efficient intermolecular packing may be affected. Due to the electron-withdrawing terminal being greatly involved in the coupling reaction, half of the end units on SMAs will be fixed or buried in the conjugated backbone of the molecular chain.[31–33] In view of their vital role in enhancing molecular packing,[34] the efficient intermolecular packings through end units will be harmed. Second, the halogen density on molecular backbone is reduced. As it is known, the introduction of halogens on molecular skeletons is one of the most effective and practical ways to regulate energy levels of SMAs, more importantly, induce more favorable intermolecular packings through noncovalent bonds or interactions.[35] At last, the great difficulty in material purification. For now, 1,1-dicyanomethylene-3-indanone (IC) and its halides are still the most widely used end units and monobrominated IC is the key to synthesizing dimers.[36] Unfortunately, due to the poor reaction selectivity, a mixture of two monobrominated isomers is afforded.[37] The quite similar polarity of isomers makes their separation and purification highly challenging. This issue not only brings troubles in synthesis but also indirectly increases the material cost, which is not conducive to the industrialization of OSCs. Accordingly, developing a new connecting approach of dimers, like branch-connected dimerized acceptors rather than terminal-connected ones,[27,38] becomes a quite promising issue.

Y. Wang, X. Jia, K. Ma, H. Liang, Z. Yao, C. Li, X. Wan, Y. Chen
State Key Laboratory of Element-Organic Chemistry
Frontiers Science Center for New Organic Matter
The Centre of Nanoscale Science and Technology and Key Laboratory of Functional Polymer Materials
Institute of Polymer Chemistry
Renewable Energy Conversion and Storage Center (RECAST)
College of Chemistry
Nankai University
Tianjin 300071, China
E-mail: zyao@nankai.edu.cn; yschen99@nankai.edu.cn
W. Zhao, G. Long
School of Materials Science and Engineering
National Institute for Advanced Materials
Renewable Energy Conversion and Storage Center (RECAST)
Nankai University
Tianjin 300350, China

The ORCID identification number(s) for the author(s) of this article can be found under https://doi.org/10.1002/marc.202400687

DOI: 10.1002/marc.202400687

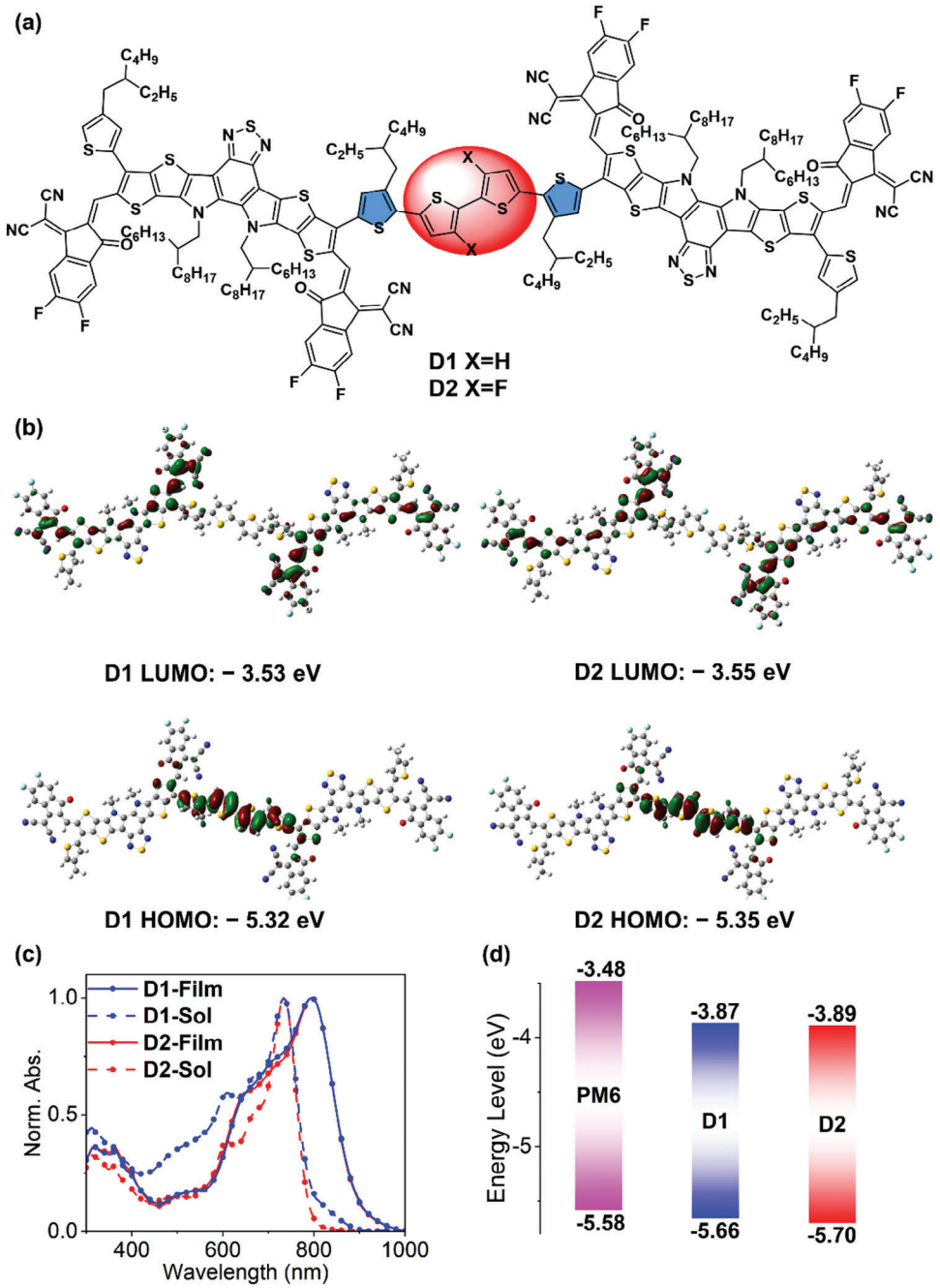

Figure 1. a) Molecular structures of D1 and D2. b) Calculated frontier molecular orbitals of D1 and D2. c) Absorption spectra of D1 and D2 in chloroform solutions and solid films. d) Energy level alignments derived from CV measurements.

With those in mind, two branch-connected dimerized acceptors, namely D1 and D2, were developed by employing bithiophene and difluorinated bithiophene as linker groups, respectively (**Figure** 1a). The fluorination on linker groups is expected to increase the intermolecular noncovalent interactions, thus inducing better intermolecular stackings and more favorable carrier transports. Therefore, the D2 acceptor affords a larger molar extinction coefficient, more importantly, a more ordered intermolecular stacking, and a clearer fiber network compared to D1. Finally, PM6:D2-based OSC yields a good PCE of 16.66%, accompanied by a good short-circuit current density (J_{SC}) of 24.33 mA cm^{-2}. On the contrary, PM6:D1-based device only shows a PCE of 15.08% and a much lower J_{SC} of 21.73 mA cm^{-2}. These achievements indicate the great significance of the linker group in constructing high-performance branch-connected dimerized acceptors and provide a promising approach for further molecular design.

2. Results and Discussion

2.1. Synthesis and Physical Properties

The synthetic routes to D1 and D2 were shown in Scheme S1 (Supporting Information), and the corresponding structural characterizations including nuclear magnetic resonance (NMR) spectra and matrix-assisted laser desorption/ionization time-of-flight (MALDI-ToF) mass spectra were displayed in Figures S14–S28 (Supporting Information). First, the monobrominated intermediate **f** was prepared based on our previously reported synthetic methods (Scheme S1, Supporting Information).[38] Immediately, **f** underwent the Stille coupling reactions with organotin of bithiophene and difluorinated bithiophene, affording two aldehyde compounds **g1** and **g2**, respectively. Lastly, 2-(5,6-difluoro-3-oxo-2,3-dihydro-1*H*-inden-1-ylidene)malononitrile (2F-IC) was employed as the end unit to deliver target D1 and D2 via fourfold Knoevenagel condensation reactions. Note that both D1 and D2 could be easily dissolved in organic solvents that are commonly used in device processing, such as chloroform and chlorobenzene.

The energy levels, distribution of frontier molecular orbitals, and molecular geometries for two dimers were first calculated by using the density functional theory method. As illustrated in Figure 1b, the lowest unoccupied molecular orbitals (LUMOs) mainly emerge along the molecular skeleton of SMAs, whereas the highest occupied molecular orbitals (HOMOs) mostly distribute on the linker groups. This suggests that the fluorination on linker groups will inevitably affect the energy levels of resulting dimerized acceptors. As expected, the large electronegativity of fluorine atoms causes the downshifting of HOMO and LUMO energy levels of D2 by ≈0.03 and 0.02 eV, respectively, compared to D1. In terms of the molecular geometries, it is worth noting that the two backbones of composed SMAs tend to be parallel in dimerized acceptors (Figure S1, Supporting Information), which may be conducive to forming the enhanced and more ordered intermolecular packings in aggregates of D1 and D2 dimerized acceptors.

UV–vis absorption spectra of D1 and D2 chloroform solutions and neat films are presented in Figure 1c. It is obvious that the maximum absorption peaks (λ_{max}) and the redshift absorptions ($\Delta\lambda$) from the solution to the thin film are almost the same for D1 and D2 (Table S1, Supporting Information). Besides, owing to the identical onset absorption (λ_{onset}), the derived optical bandgaps (E_g^{opt}) are also equal for D1 and D2 films. As shown in Figure S2 (Supporting Information), both dimers exhibit a slight blueshift at the maximum absorption peak from 20 to 100 °C, ≈5 nm, which indicates the similar molecular interactions and aggregation behavior of these acceptors in chlorobenzene. This may be due to their almost identical conjugated skeleton. However, the molar extinction coefficient (ϵ_{max}) of D2 is estimated as 3.04×10^5 L mol^{-1} cm^{-1} while that of D1 is only 2.87×10^5 L mol^{-1} cm^{-1} (Figure S3, Supporting Information). This indicates that D2 has the more powerful light harvesting ability, which should be advantageous for obtaining higher J_{SC} in OSCs. The experimental HOMO and LUMO energy levels of D1 and D2 were estimated by resorting to cyclic voltammograms (CV) measurements (Figure S4, Supporting Information). As exhibited in Figure 1d, the HOMO energy levels of D1 and D2 are −5.66 and −5.70 eV, while the LUMOs are −3.87 and −3.89 eV, respectively. The relative arrangements of energy levels are consistent with the results predicted by the DFT method. In theory, the downshift of the HOMO energy level of D2, which is caused by fluorination on linker groups, will provide more driving force for exciton dissociation at the D/A interface.

2.2. Photovoltaic Performance

Given the complementary absorption and well-matched energy levels (Figure S5, Supporting Information), PM6 was selected as the donor and mixed with D1 and D2 to compose OSCs with a structure of ITO/PEDOT:PSS/PM6:D1 (or PM6:D2)/PNDIT-F3N/Ag.[39] The structures of PNDIT-F3N and PM6 are shown in Figure S6 (Supporting Information). Then, the careful optimization of the weight ratio of donor and acceptor, post-thermal-annealing treatment, and the ratio of additive were conducted and the detailed device parameters were listed in Tables S2 and S3 (Supporting Information). Among them, the best *J*–*V* curves for D1 and D2-based devices were presented in **Figure 2a** and the derived photovoltaic data were enumerated in **Table 1**. The OSCs based on D2 achieved a superior PCE of 16.66%, accompanied by an open-circuit voltage (V_{OC}) of 0.876 V, a J_{SC} of 24.33 mA cm^{-2} and a fill factor (FF) of 78.17%. As a comparison, the device based on D1 only obtained a modest PCE of 15.08% with a V_{OC} of 0.887 V, a J_{SC} of 21.73 mA cm^{-2} and an FF of 78.61%. The potential reason for the slightly lower V_{OC} of D2-based devices is the deeper LUMO energy level of D2, considering that the V_{OC} is roughly in proportion to the energy offset of the HOMO of donors versus the LUMO of acceptors.[40–42]

The external quantum efficiencies (EQEs) are also shown in Figure 2b. Despite the similar photoelectron response ranges, the fully improved EQEs for D2-based OSCs have contributed to a much larger integrated J_{SC}. As expected, the integrated J_{SC}s obtained from the devices based on D1 and D2 are 20.75 and 23.35 mA cm^{-2}, respectively. It is worth noting that EQEs are typically influenced by various ingredients,[43–45] herein, the improved EQEs and PCEs for D2-based OSCs should attributed to both the enhanced light-harvesting ability (Figure S7, Supporting Information) and fluorine-induced better charge transfer/transport processes (discussed below) in D2 blended films.

2.3. Charge Dynamics and Energy Loss Analysis

In order to uncover the charge generation and collection changes in two devices, the dependence of photocurrent density (J_{ph}) on the effective voltage (V_{eff}) was characterized and displayed in Figure 2c. The ratios of J_{SC} under short-circuit condition/saturation current density (J_{sat}) and J_{SC} under maximum output condition/J_{sat} could reflect the exciton dissociation efficiency (P_{diss}) and charge collection efficiency (P_{coll}) of OSCs, respectively.[46] As a result, the D2-based device achieved the P_{diss} and P_{coll} values of 98.01% and 89.39%, respectively, which are larger than those of D1-based devices (97.12% and 86.61%, respectively). Moreover, the higher photoluminescence quenching yield of 89.45% for the D2-based device, compared with

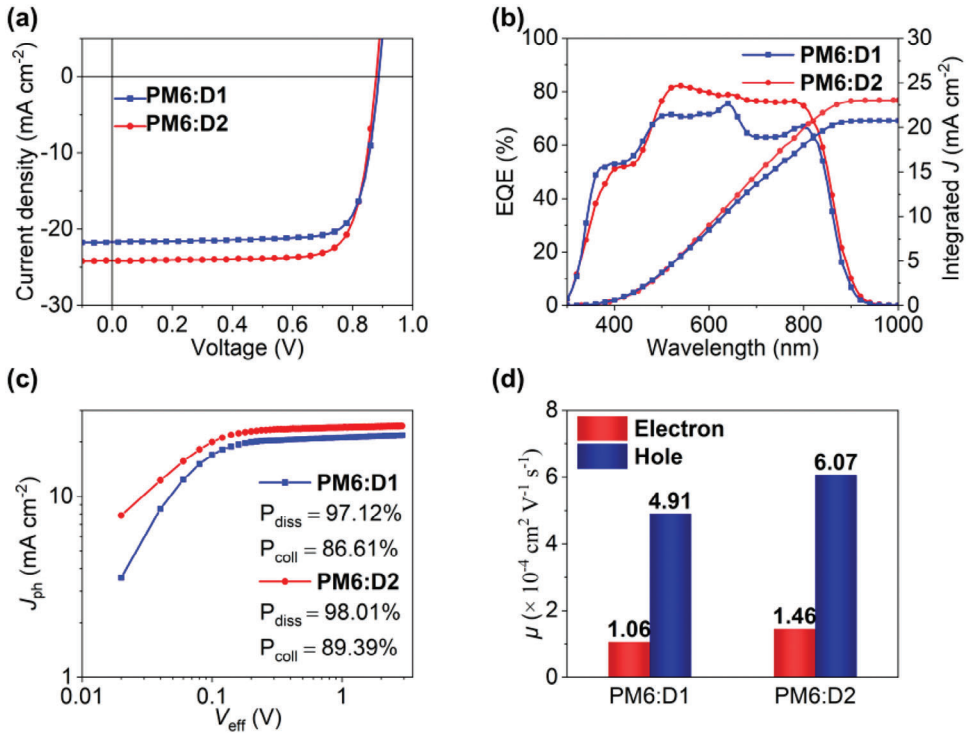

Figure 2. a) J–V curves for OSCs. b) EQE plots and integrated J_{SC} curves. c) J_{ph} versus V_{eff} curves indicating P_{diss} and P_{coll}. d) Hole and electron mobilities of PM6:D2 and PM6:D1 based devices.

that of 80.35% for the D1-based device, also proves its superior exciton dissociation of D2-based OSC (Figure S8, Supporting Information). The higher P_{diss} and P_{coll} values should account for the increased EQEs and J_{SC} of D2-based OSCs, as it has been mentioned above. Furthermore, the space-charge-limited current (SCLC) method was used to examine the electron (μ_e) and hole (μ_h) mobilities for D1, D2, and their blended films (Figure 2d; Figure S9 and Table S6, Supporting Information).[47–49] The μ_es for D1 and D2 neat films are 4.19×10^{-4} and 5.17×10^{-4} cm^2 V^{-1} s^{-1}, respectively. Moreover, the μ_e/μ_h for blended films could be confirmed as $1.46 \times 10^{-4}/6.07 \times 10^{-4}$ cm^2 V^{-1} s^{-1} for D2 and $1.06 \times 10^{-4}/4.91 \times 10^{-4}$ for D1. Notably, the slightly improved charge carrier mobilities for D2 can be attributed to its superior film morphology, which is induced by fluorination on linker groups.

To further elucidate the difference in V_{OC} between the two devices, a detailed energy losses (E_{loss}) analysis was conducted (Table S7, Supporting Information).[50–52] The optical bandgaps (E_g) of blended films were estimated by the derivatives of EQE curves (Figure S10, Supporting Information), being 1.446 and 1.438 eV for D1- and D2-based OSCs, respectively. Inferred from the equation of $E_{loss} = E_g - qV_{OC}$ (where q is the elementary charge), the corresponding E_{loss} for D1- and D2-based OSCs are 0.591 and 0.611 eV, respectively. In detail, the values of ΔE_1 (radiative recombination loss above the bandgap) of D1 and D2-based OSCs are 0.261 and 0.266 eV, respectively. The second parts (ΔE_2, radiative recombination loss below the bandgap) are 0.087 eV for D1 and 0.091 eV for D2. Then, the last parts of ΔE_3 (non-radiative energy loss) for D1 and D2 are 0.243 and 0.254 eV according to the equation of $\Delta E_3 = -kT\ln(EQE^{EL})$,[53–55] where k is the Boltzmann constant and T represents the Kelvin temperature. This is consistent with the photoluminescence quantum yield results in Figure S11 (Supporting Information). Generally, fluorination on linker groups of dimerized acceptors seems to have no obvious effects on the energy losses in resulting OSCs. Besides, the Urbach energies (E_U) for D1 and D2 blended films were also measured, being 53.81 and 53.55 meV, respectively (Figure S12, Supporting Information).[56–58] The nearly identical E_Us are consistent with similar energy losses for D1- and D2-based OSCs.

Table 1. Summary of photovoltaic parameters for OSCs.

Active Layers	V_{OC} [V]	J_{SC} [mA cm^{-2}]	Cal. J_{SC}[a)] [mA cm^{-2}]	FF [%]	PCE [%][b)]
PM6:D1	0.887	21.73	20.75	78.61	15.08
	(0.879 ± 0.010)	(21.64 ± 0.46)		(78.03 ± 0.96)	(14.90 ± 0.24)
PM6:D2	0.876	24.33	23.35	78.17	16.66
	(0.877 ± 0.004)	(24.15 ± 0.22)		(78.26 ± 0.26)	(16.56 ± 0.10)

[a)] Current densities by integrating EQE plots. [b)] Average parameters derived from 15 independent OSCs (Tables S4 and S5, Supporting Information);

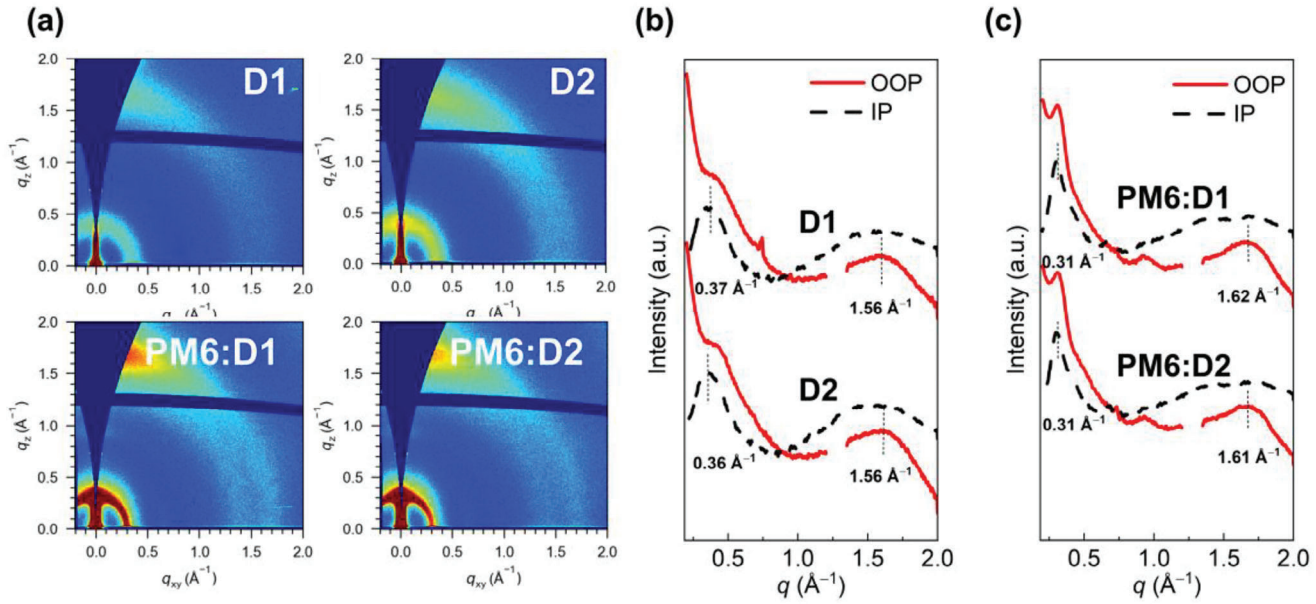

Figure 3. a) 2D GIWAXS patterns of neat films and blended films. Extracted line-cut profiles from 2D GIWAXS patterns of b) neat films and c) blended films.

2.4. Morphology Analysis

As we have discussed above, the higher J_{SC} of D2-based devices may be ascribed to a superior nanoscale bulk heterojunction (BHJ) morphology in active layers.[59] Thus, we further resorted to the grazing incident wide-angle X-ray scattering (GIWAXs) measurement, to elucidate the molecular crystallinity, and packing orientations of D1 and D2 (**Figure 3a**; Table S8, Supporting Information).[60] The predominant face-on orientation can be observed in both D1 and D2 neat films since both of them showed the evident (010) peaks at 1.56 Å^{-1} in the out-of-plane (OOP) direction (Figure 3b), moreover, indicating the similar π–π stacking distance of 4.03 Å. However, whether in the OOP or in-plane (IP) directions, an enlarged crystal coherence length (CCL) can be observed for D2 (37.68 Å in OOP and 28.26 Å in IP) compared to D1 (29.75 Å for OOP and 25.69 Å for IP), indicating the superior crystalline ordering in D2 neat films. What's more, although the π–π stacking distance in two blended films is semblable (≈3.89 Å, Figure 3c), an enlarged CCL (29.75 Å) for PM6:D2 compared to that of PM6:D1 (23.55 Å) still reveals the more ordered intermolecular packing in D2 films, which should be induced by the fluorination on linker groups.

Atomic force microscopy (AFM) and AFM-based infrared spectroscopy (AFM-IR) were also employed to characterize the

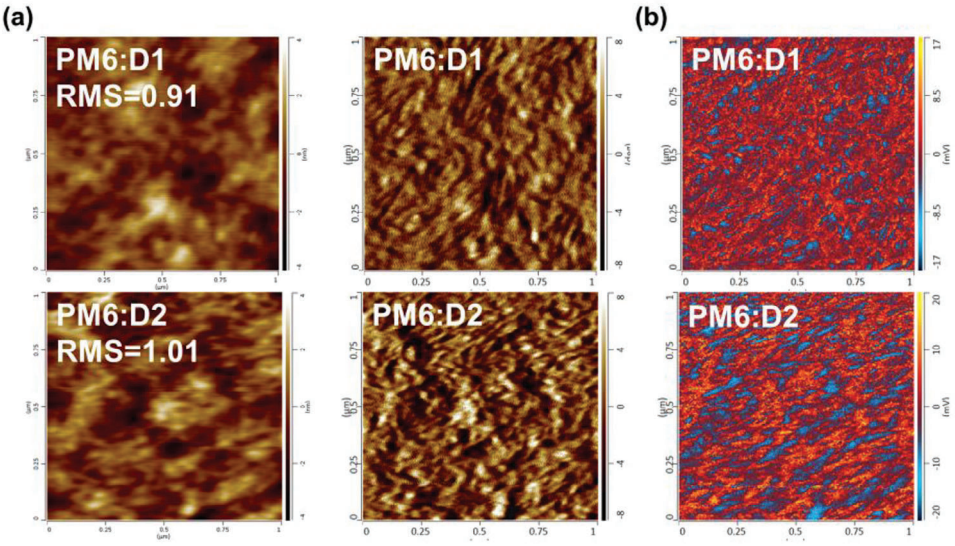

Figure 4. a) AFM and b) AFM-IR images of blended films.

surface morphologies of PM6:D1 and PM6:D2 blended films. As shown in **Figure 4a**, both the blended films exhibited smooth and uniform surfaces with root-mean-square values of 0.91 nm for PM6:D1 and 1.01 nm for PM6:D2. More importantly, PM6:D2 blend possesses a better fibrillary morphology compared to PM6:D1, which in theory could facilitate charge transport.[61] This phenomenon could be confirmed by the AFM-IR images (Figure 4b, blue and red colors represent PM6 and acceptor, respectively). The IR spectra of D1, D2, and PM6 are shown in Figure S13 (Supporting Information). Markedly, more pronounced acceptor domains were discovered in PM6:D2 blended film. Theoretically speaking, the desirable morphology in PM6:D2 blended films is closely related to its better charge transfer/transport dynamics and even determines the better photovoltaic performance of PM6:D2-based OSCs.

3. Conclusion

Two branch-connected dimerized acceptors, namely D1 and D2, were developed by employing bithiophene and difluorinated bithiophene as linker groups, respectively. After an in-depth analysis, it has been revealed that D2, which benefits from the fluorination on linker groups, possesses a larger molar extinction coefficient, better molecular planarity, more ordered intermolecular packing, and superior charge transport behavior compared to that D1. Subsequently, when blending with a suitable donor PM6, the favorable face-on molecular packing orientation and better crystalline ordering of D2 can be remained in blended films, providing an enhanced fibrillary network with respect to that of D1. As a consequence, D2-based OSCs reached an excellent PCE of 16.66% with a significantly higher J_{SC} than D1-based ones. Our work demonstrates the great significance of linker group screening in constructing high-performance branch-connected dimerized acceptors and will stimulate more efforts to explore highly efficient dimerized SMAs through delicately linker group design.

4. Experimental Section

Experimental methods are available in the Supporting Information.

Supporting Information

Supporting Information is available from the Wiley Online Library or from the author.

Acknowledgements

Y.W. and X.J. equally contributed to this work. The authors gratefully acknowledge the financial support from the MoST of China (2022YFB4200400, 2023YFE0210400, 2019YFA0705900, and 2022YFA1203304), the NSFC (21935007, 22361132530, 52025033, and 52373189), and the Tianjin city (23JCZDJC01160).

Conflict of Interest

The authors declare no conflict of interest.

Data Availability Statement

The data that support the findings of this study are available from the corresponding author upon reasonable request.

Keywords

connecting method, dimerized acceptor molecules, fluorination, organic solar cells

Received: August 28, 2024
Revised: October 19, 2024
Published online:

[1] O. Inganäs, *Adv. Mater.* **2018**, *30*, 1800388.
[2] H. Yao, J. Hou, *Angew. Chem., Int. Ed.* **2022**, *61*, e202209021.
[3] J. Cao, L. Yi, L. Zhang, Y. Zou, L. Ding, *J. Mater. Chem. A* **2023**, *11*, 17.
[4] S. Li, Z. Li, X. Wan, Y. Chen, *eScience* **2023**, *3*, 100085.
[5] C. Chen, L. Wang, W. Xia, K. Qiu, C. Guo, Z. Gan, J. Zhou, Y. Sun, D. Liu, W. Li, T. Wang, *Nat. Commun.* **2024**, *15*, 6865.
[6] Y. Jiang, S. Sun, R. Xu, F. Liu, X. Miao, G. Ran, K. Liu, Y. Yi, W. Zhang, X. Zhu, *Nat. Energy* **2024**, *9*, 975.
[7] S. Guan, Y. Li, C. Xu, N. Yin, C. Xu, C. Wang, M. Wang, Y. Xu, Q. Chen, D. Wang, L. Zuo, H. Chen, *Adv. Mater.* **2024**, *36*, 2400342.
[8] Z. Chen, J. Ge, W. Song, X. Tong, H. Liu, X. Yu, J. Li, J. Shi, L. Xie, C. Han, Q. Liu, Z. Ge, *Adv. Mater.* **2024**, *36*, 2406690.
[9] H. Lu, D. Li, W. Liu, G. Ran, H. Wu, N. Wei, Z. Tang, Y. Liu, W. Zhang, Z. Bo, *Angew. Chem., Int. Ed.* **2024**, *63*, e202407007.
[10] H. Hu, L. Ye, M. Ghasemi, N. Balar, J. J. Rech, S. J. Stuard, W. You, B. T. O'Connor, H. Ade, *Adv. Mater.* **2019**, *31*, 1808279.
[11] Y. Dong, Y. Zou, J. Yuan, H. Yang, Y. Wu, C. Cui, Y. Li, *Adv. Mater.* **2019**, *31*, 1904601.
[12] J. Luke, E. J. Yang, C. Labanti, S. Y. Park, J.-S. Kim, *Nat. Rev. Mater.* **2023**, *8*, 839.
[13] S. Li, R. Zhang, M. Zhang, J. Yao, Z. Peng, Q. Chen, C. Zhang, B. Chang, Y. Bai, H. Fu, Y. Ouyang, C. Zhang, J. A. Steele, T. Alshahrani, M. B. J. Roeffaers, E. Solano, L. Meng, F. Gao, Y. Li, Z.-G. Zhang, *Adv. Mater.* **2023**, *35*, 2206563.
[14] Y. Bai, Z. Zhang, Q. Zhou, H. Geng, Q. Chen, S. Kim, R. Zhang, C. Zhang, B. Chang, S. Li, H. Fu, L. Xue, H. Wang, W. Li, W. Chen, M. Gao, L. Ye, Y. Zhou, Y. Ouyang, C. Zhang, F. Gao, C. Yang, Y. Li, Z.-G. Zhang, *Nat. Commun.* **2023**, *14*, 2926.
[15] M. Ghasemi, H. Hu, Z. Peng, J. J. Rech, I. Angunawela, J. H. Carpenter, S. J. Stuard, A. Wadsworth, I. McCulloch, W. You, H. Ade, *Joule* **2019**, *3*, 1328.
[16] G. Sun, X. Jiang, X. Li, L. Meng, J. Zhang, S. Qin, X. Kong, J. Li, J. Xin, W. Ma, Y. Li, *Nat. Commun.* **2022**, *13*, 5267.
[17] Z.-G. Zhang, Y. Li, *Angew. Chem., Int. Ed.* **2021**, *60*, 4422.
[18] Z.-G. Zhang, Y. Yang, J. Yao, L. Xue, S. Chen, X. Li, W. Morrison, C. Yang, Y. Li, *Angew. Chem., Int. Ed.* **2017**, *56*, 13503.
[19] T. Chen, X. Zheng, D. Wang, Y. Zhu, Y. Ouyang, J. Xue, M. Wang, S. Wang, W. Ma, C. Zhang, Z. Ma, S. Li, L. Zuo, H. Chen, *Adv. Mater.* **2024**, *36*, 2308061.
[20] Z. Wang, X. Wang, L. Tu, H. Wang, M. Du, T. Dai, Q. Guo, Y. Shi, E. Zhou, *Angew. Chem., Int. Ed.* **2024**, *63*, e202319755.
[21] J. Wang, Y. Li, C. Han, L. Chen, F. Bi, Z. Hu, C. Yang, X. Bao, J. Chu, *Energy Environ. Sci.* **2024**, *17*, 4216.
[22] Q. Fan, Q. An, Y. Lin, Y. Xia, Q. Li, M. Zhang, W. Su, W. Peng, C. Zhang, F. Liu, L. Hou, W. Zhu, D. Yu, M. Xiao, E. Moons, F. Zhang, T. D. Anthopoulos, O. Inganäs, E. Wang, *Energy Environ. Sci.* **2020**, *13*, 5017.

[23] Z. Luo, T. Liu, R. Ma, Y. Xiao, L. Zhan, G. Zhang, H. Sun, F. Ni, G. Chai, J. Wang, C. Zhong, Y. Zou, X. Guo, X. Lu, H. Chen, H. Yan, C. Yang, **2020**, *32*, 2005942.
[24] W. Wang, Q. Wu, R. Sun, J. Guo, Y. Wu, M. Shi, W. Yang, H. Li, J. Min, *Joule* **2020**, *4*, 1070.
[25] Y. Bai, T. Chen, X. Ji, J. Wang, W. Zhao, S. Yuan, Y. Zhang, G. Long, Z. Zhang, X. Wan, B. Kan, Y. Chen, *Adv. Energy Mater.* **2024**, *14*, 2400938.
[26] X. Meng, M. Li, K. Jin, L. Zhang, J. Sun, W. Zhang, C. Yi, J. Yang, F. Hao, G.-W. Wang, Z. Xiao, L. Ding, *Angew. Chem., Int. Ed.* **2022**, *61*, e202207762.
[27] F. Yi, M. Xiao, Y. Meng, H. Bai, W. Su, W. Gao, Z.-F. Yao, G. Qi, Z. Liang, C. Jin, L. Tang, R. Zhang, L. Yan, Y. Liu, W. Zhu, W. Ma, Q. Fan, *Angew. Chem., Int. Ed.* **2024**, *63*, e202319295.
[28] H. Zhuo, X. Li, J. Zhang, C. Zhu, H. He, K. Ding, J. Li, L. Meng, H. Ade, Y. Li, *Nat. Commun.* **2023**, *14*, 7996.
[29] H. Zhuo, X. Li, J. Zhang, S. Qin, J. Guo, R. Zhou, X. Jiang, X. Wu, Z. Chen, J. Li, L. Meng, Y. Li, *Angew. Chem., Int. Ed.* **2023**, *62*, e202303551.
[30] F. Qi, Y. Li, R. Zhang, F. R. Lin, K. Liu, Q. Fan, A. K.-Y. Jen, *Angew. Chem., Int. Ed.* **2023**, *62*, e202303066.
[31] Z. Zhang, S. Yuan, T. Chen, J. Wang, Y.-Q.-Q. Yi, B. Zhao, M. Li, Z. Yao, C. Li, X. Wan, G. Long, B. Kan, Y. Chen, *Energy Environ. Sci.* **2024**, *17*, 5719.
[32] H. Chen, Z. Zhang, P. Wang, Y. Zhang, K. Ma, Y. Lin, T. Duan, T. He, Z. Ma, G. Long, C. Li, B. Kan, Z. Yao, X. Wan, Y. Chen, *Energy Environ. Sci.* **2023**, *16*, 1773.
[33] H. Chen, B. Kan, P. Wang, W. Feng, L. Li, S. Zhang, T. Chen, Y. Yang, T. Duan, Z. Yao, C. Li, X. Wan, Y. Chen, *Angew. Chem., Int. Ed.* **2023**, *62*, e202307962.
[34] Z. Yao, X. Cao, X. Bi, T. He, Y. Li, X. Jia, H. Liang, Y. Guo, G. Long, B. Kan, C. Li, X. Wan, Y. Chen, *Angew. Chem., Int. Ed.* **2023**, *62*, e202312630.
[35] H. Liang, X. Bi, H. Chen, T. He, Y. Lin, Y. Zhang, K. Ma, W. Feng, Z. Ma, G. Long, C. Li, B. Kan, H. Zhang, O. A. Rakitin, X. Wan, Z. Yao, Y. Chen, *Nat. Commun.* **2023**, *14*, 4707.
[36] X. Yang, Y. Gao, L.-Y. Xu, X. Wu, X. Chen, Y. Shao, B. Xiao, S. Liu, J. Xia, R. Sun, J. Min, *Energy Environ. Sci.* **2024**, *17*, 5962.
[37] Z. Luo, T. Liu, R. Ma, Y. Xiao, L. Zhan, G. Zhang, H. Sun, F. Ni, G. Chai, J. Wang, C. Zhong, Y. Zou, X. Guo, X. Lu, H. Chen, H. Yan, C. Yang, *Adv. Mater.* **2020**, *32*, 2005942.
[38] K. Ma, H. Liang, Y. Wang, T. He, T. Duan, X. Si, W. Shi, G. Long, X. Cao, Z. Yao, X. Wan, C. Li, B. Kan, Y. Chen, *Sci. China: Chem.* **2024**, *67*, 1687.
[39] M. Zhang, X. Guo, W. Ma, H. Ade, J. Hou, *Adv. Mater.* **2015**, *27*, 4655.
[40] S. Zhang, Y. Qin, J. Zhu, J. Hou, *Adv. Mater.* **2018**, *30*, 1800868.
[41] Z. Fei, F. D. Eisner, X. Jiao, M. Azzouzi, J. A. Röhr, Y. Han, M. Shahid, A. S. R. Chesman, C. D. Easton, C. R. McNeill, T. D. Anthopoulos, J. Nelson, M. Heeney, *Adv. Mater.* **2018**, *30*, 1800728.
[42] T. J. Aldrich, M. Matta, W. Zhu, S. M. Swick, C. L. Stern, G. C. Schatz, A. Facchetti, F. S. Melkonyan, T. J. Marks, *J. Am. Chem. Soc.* **2019**, *141*, 3274.
[43] F. Bai, J. Zhang, A. Zeng, H. Zhao, K. Duan, H. Yu, K. Cheng, G. Chai, Y. Chen, J. Liang, W. Ma, H. Yan, *Joule* **2021**, *5*, 1231.
[44] Y. Liu, Z. Zheng, V. Coropceanu, J.-L. Brédas, D. S. Ginger, *Mater. Horiz.* **2022**, *9*, 325.
[45] R. Sun, W. Wang, H. Yu, Z. Chen, X. Xia, H. Shen, J. Guo, M. Shi, Y. Zheng, Y. Wu, W. Yang, T. Wang, Q. Wu, Y. Yang, X. Lu, J. Xia, C. J. Brabec, H. Yan, Y. Li, J. Min, *Joule* **2021**, *5*, 1548.
[46] N. Gasparini, M. Salvador, S. Strohm, T. Heumueller, I. Levchuk, A. Wadsworth, J. H. Bannock, J. C. de Mello, H.-J. Egelhaaf, D. Baran, I. McCulloch, C. J. Brabec, *Adv. Energy Mater.* **2017**, *7*, 1700770.
[47] H. Azimi, A. Senes, M. C. Scharber, K. Hingerl, C. J. Brabec, *Adv. Energy Mater.* **2011**, *1*, 1162.
[48] F. Schauer, *Sol. Energy Mater. Sol. Cells* **2005**, *87*, 235.
[49] P. N. Murgatroyd, *J. Phys. D: Appl. Phys.* **1970**, *3*, 151.
[50] H.-S. Yang, D. Kim, C.-M. Oh, V. Tamilavan, P. M. Hangoma, H. Yi, B. R. Lee, I. Shin, I.-W. Hwang, S. H. Park, *Carbon Energy* **2024**, *6*, e433.
[51] G. Zhang, F. R. Lin, F. Qi, T. Heumüller, A. Distler, H.-J. Egelhaaf, N. Li, P. C. Y. Chow, C. J. Brabec, A. K. Y. Jen, H.-L. Yip, *Chem. Rev.* **2022**, *122*, 14180.
[52] X. Wu, C. Gao, Q. Chen, Y. Yan, G. Zhang, T. Guo, H. Chen, *Nat. Commun.* **2023**, *14*, 1579.
[53] C. Li, J. Zhou, J. Song, J. Xu, H. Zhang, X. Zhang, J. Guo, L. Zhu, D. Wei, G. Han, J. Min, Y. Zhang, Z. Xie, Y. Yi, H. Yan, F. Gao, F. Liu, Y. Sun, *Nat. Energy* **2021**, *6*, 605.
[54] Y. Shi, Y. Chang, K. Lu, Z. Chen, J. Zhang, Y. Yan, D. Qiu, Y. Liu, M. A. Adil, W. Ma, X. Hao, L. Zhu, Z. Wei, *Nat. Commun.* **2022**, *13*, 3256.
[55] S. Liu, J. Yuan, W. Deng, M. Luo, Y. Xie, Q. Liang, Y. Zou, Z. He, H. Wu, Y. Cao, *Nat. Photonics* **2020**, *14*, 300.
[56] H. Liu, M. Li, H. Wu, J. Wang, Z. Ma, Z. Tang, *J. Mater. Chem. A* **2021**, *9*, 19770.
[57] J. Yuan, C. Zhang, B. Qiu, W. Liu, S. K. So, M. Mainville, M. Leclerc, S. Shoaee, D. Neher, Y. Zou, *Energy Environ. Sci.* **2022**, *15*, 2806.
[58] J. Liu, S. Chen, D. Qian, B. Gautam, G. Yang, J. Zhao, J. Bergqvist, F. Zhang, W. Ma, H. Ade, O. Inganäs, K. Gundogdu, F. Gao, H. Yan, *Nat. Energy* **2016**, *1*, 16089.
[59] Z. Wang, Y. Zhang, J. Zhang, Z. Wei, W. Ma, *Adv. Energy Mater.* **2016**, *6*, 1502456.
[60] H. Alexander, B. Wim, G. James, S. Eric, G. Eliot, K. Rick, M. Alastair, C. Matthew, R. Bruce, P. Howard, *J. Phys.: Conf. Ser.* **2010**, *247*, 012007.
[61] G. Zhang, X. Xu, Z. Bi, W. Ma, D. Tang, Y. Li, Q. Peng, *Adv. Funct. Mater.* **2018**, *28*, 1706404.